Photocurable Printed Piezocapacitive Pressure Sensor Based on an Acrylic Resin Modified with Polyaniline and Lignin

Goretti Arias-Ferreiro, Ana Ares-Pernas, Aurora Lasagabáster-Latorre, M. Sonia Dopico-García, Pablo Ligero, N. Pereira, P. Costa, S. Lanceros-Mendez, and María-José Abad*

The design of suitable materials for the manufacture of pressure sensors with high sensitivity and flexibility in wearable electronics is still a challenge. In this study, a flexible and portable pressure sensor is developed based on a photopolymeric formulation of polyaniline (PANI)/Lignin/acrylate. The amount of photoinitiator and the presence of lignin within the filler are investigated to obtain the best printability and capacitive response. Low PANI contents drastically increase the dielectric constant and 4 wt% photoinitiator improves the signal and sensitivity. A sensitivity of 0.012 kPa^{-1} is achieved in a linear range (0–10 kPa) with only 3.5 wt% PANI. Lignin improves both the dispersion of the filler within the matrix and the printability of the resin, due to lower absorptivity at the UV wavelength of the 3D printer. Thus, the PANI-Lignin filler is selected for the fabrication of a piezocapacitive prototype transducer. The pressure transducer demonstrate its practical application by responding to a human footfall and transmitting its corresponding electrical signal. This study shows the enhanced properties of lignin modified PANI acrylate composites. Based on lignin, an abundant natural waste, a sustainable photocurable cost-effective polymer is proposed for the fabrication of printable, wearable electronics.

1. Introduction

Society increasingly claims for smart and multifunctional materials in order to satisfy the demand for digitalization, including the sensing of production processes (Industry 4.0) and increased interactivity (Internet of Things).[1] In this context, dielectric polymeric materials are being investigated due to their scientific and technological interest since they combine dielectric properties with appropriate mechanical flexibility and simple processability.[2,3] Such composite materials show huge opportunities to be integrated in devices such as electronics,[4–6] sensors and actuators.[7]

Within this context, additive manufacturing emerges as a set of advanced fabrication techniques that enable the production of fully functional electronic devices in one step printing.[1,8–10] However, for photopolymerization-based 3D printing techniques the number of UV curable materials suitable for the fabrication of sensors and actuators is still scarce.[1] Research in this field pursues 3D printing materials with new features but also environmentally more friendly and sustainable, as demanded by today's society.[11–13] Techniques as stereolithography (SLA) and digital light processing (DLP) are based on the layer-by-layer solidification of a liquid photosensitive resin via UV-light exposure.[14] This is a tailorable process where multicomponent resins provide the photo-rheological and mechanical properties necessary to ensure a successful print.[15]

G. Arias-Ferreiro, A. Ares-Pernas, M. S. Dopico-García, M.-J. Abad
Universidade da Coruña
Campus Industrial de Ferrol
Grupo de Polímeros-CIT
Campus de Esteiro
Ferrol 15403, Spain
E-mail: mjabad@udc.es
A. Lasagabáster-Latorre
Dpto Química Orgánica I
Facultad de Óptica
Universidad Complutense de Madrid
Arcos de Jalón 118, Madrid 28037, Spain

P. Ligero
Enxeñería Química Ambiental Group
Centro de Investigacións Científicas Avanzadas (CICA)
Universidade da Coruña
A Coruña 15071, Spain
N. Pereira, P. Costa
Centro de Física
Universidade do Minho
Braga 4710-057, Portugal
S. Lanceros-Mendez
IKERBASQUE
Basque Foundation for Science
Bilbao 48009, Spain
S. Lanceros-Mendez
BCMaterials
Basque Center for Materials
Applications and Nanostructures
UPV/EHU Science Park, Leioa 48940, Spain

**ADVANCED
SCIENCE NEWS**
www.advancedsciencenews.com

**ADVANCED
MATERIALS
TECHNOLOGIES**
www.advmattechnol.de

By using these technologies with appropriated materials it is possible to develop functional and multifunctional devices and components. Pressure sensor is a specific electronic device that converts pressure into the corresponding electrical signal.[16] Capacitive pressure sensors attract higher interest compared to other types of sensors such as resistive or piezoelectric ones due to their simple structure, low fabrication costs and low power consumption.[17–19] A capacitive pressure sensor consists of a dielectric layer placed between two parallel electrodes. There are several application modes of those sensors; one of the most implemented includes the variation of the thickness of the sensor dielectric layer under an applied force, leading to the variation of the capacitance of the sensor. Consequently, a highly deformable dielectric layer is a critical component for improving the sensitivity of capacitive pressure sensors.[19]

Polyaniline is an excellent candidate for fabricating sensor devices,[20–22] energy conversion and storage systems or supercapacitors due to its intrinsic electrical properties,[23–25] together with good environmental stability, simple synthesis and low cost.[26] Its use in capacitive sensors has been recently investigated [20,21] with scarce applications in flexible devices,[22] compared to the broad investigation of other materials such as carbon nanotubes, Au, Ag, or Cu particles.[16] Therefore, as far as the authors are aware, there are no studies dedicated to the synthesis of flexible materials, suitable for conventional 3D printing (DLP) based on polyaniline (PANI) in a photocurable acrylic matrix, valid for wearable electronics and sensors fabrication. The addition of polyanilines to UV curable resins [27–29] for 3D printing [30,31] is a major challenge due to the high UV absorption of PANI, so the investigation of this topic represents a significant scientific and technological novelty.

From another point of view, the demand for sustainable functional materials with an ecological preparation process is boosting due to the problems caused by petroleum based products. Lignin is a complex aromatic heteropolymer and the second most abundant biopolymer on earth. Considering the merits of excellent biodegradation, low cost, and environmental friendliness, lignin exhibits potential application for the preparation of high value sustainable materials.[32–34]

Its use in additive manufacturing is an emerging field[15] and has been introduced recently into bio-feedstocks as a reinforcing or nucleating agent, filler or antioxidant to enhance the performance of 3D printed objects,[35] mainly by fused deposition modelling (FDM). Only a few reports deal with the addition of lignin in resin formulations for stereolitography.[36–39] Furthermore, lignin has high potential in electronic applications, such as energy storage and conversion, as well as in other areas for instance pollutant removal.[40,41] When lignin is incorporated into electroactive materials (such as polyaniline), the redox activity of the quinone/hidroquinone structures allows the charge storage capacity to be improved.[42] The hybrid structure of conjugated polymer/lignin provides both electronic conductivity and quinone redox activity.[43] Polyaniline-lignin composites with interpenetrating fibrous networks have been obtained by in situ polymerization of aniline using reticulated lignin as the framework, obtaining a composite with improved capacity.[44] Thereby, it seems possible to improve the properties of the composite, while taking advantage of a very abundant

natural waste, thus achieving a more environmentally friendly photocurable polymeric mixture.

The main target of this work is the development of a novel photocurable printed piezocapacitive sensor made of an eco-friendly resin, suitable for digital light processing (DLP), using polyaniline modified with lignin (PANI-L) as filler. The present work continues previous research in which PANI was incorporated as a conductive filler [45] into an in-house formulated resin by means of a solvent-free, bulk photopolymerization process. The resin is compounded by ethyleneglycolphenylether acrylate (EGPEA) as principal monomer, 1,6-hexanediol diacrylate (HDODA) as crosslinker, and diphenyl (2,4,6-trimethylbenzoyl) phosphine oxide (TPO) as photoinitiator.[29] The crosslinker and conductive filler concentrations were adjusted in the previous study. In particular, the present work reports on the effect of the amount of photoinitiator and the presence of lignin in order to obtain the best capacitive response and printability of the acrylic resin.

Flexible rectangular and dog-bone shaped specimens samples of the different acrylic composites have been successfully printed following the procedure described in section 4. The systematic study and physical-chemical characterization of the 3D printed films revealed that low filler contents dramatically increased the dielectric constant (ε' >30) and that the lowest concentration of TPO assayed enhanced the signal and sensibility of a capacitive sensor. Further, the introduction of PANI-L filler, with lower viscosity and UV absorptivity, improved the dispersion of the filler particles within the matrix, the photocuring performance and printability of the resin. The data obtained provides valuable guidance for the development of new printable, cost-effective composites containing PANI-L as filler, thus allowing a more ecofriendly, solvent-free process for the fabrication of piezocapacitive sensors. As an example of applicability, a piezocapacitive potential prototype sensor was printed and tested using the PANI-L acrylic composite.

2. Results and Discussion

2.1. Viscosity of Liquid Formulations

The effect of photoinitiator and conductive filler concentrations on the viscosity of the liquid formulations were studied at room temperature, as shown in Figure S1A and B. The adequate viscosity of the resin is key to ensure a successful printing process.[4,46] The viscosity values obtained at 10 s^{-1} for all formulations are summarized in **Table 1**.

A clear increase in viscosity was observed with increasing PANI concentration. The presence of PANI disturbed the normal flow of the polymer; consequently, the viscosity of the formulation augmented from 0.005 Pa s to 0.022 Pa s at 10 s^{-1} as the PANI loadings increased from 0 to 3.5% by weight. These values represent an order of magnitude increase. Additionally, it is important to note that the presence of lignin in the pure resin did not produce a significant change in the viscosity values (T4L04). However, when PANI-L was used instead of PANI with a 3.5 wt% filler content, this value diminished to 0.011 Pa.s, only half of the expected value. So, the presence of lignin in the filler (PANI-L) decreased the viscosity of the resin

**ADVANCED
SCIENCE NEWS**

www.advancedsciencenews.com

**ADVANCED
MATERIALS
TECHNOLOGIES**

www.advmattechnol.de

Table 1. Theoretical (T) and experimental content of PANI, PANI-L or Lignin in the samples obtained by elemental analysis (EA), viscosity values at 10 s^{-1} of composites and double bond conversion (DBC %).

Sample	Filler (T) (wt%)	Filler (EA) (wt%)	Viscosity (Pa.s) at 10 s^{-1}	DBC (%)
T4P0	0	<0.05	0.005	97.9 ± 0.7
T4L04	0.4	-	0.006	97.0 ± 0.8
T4P1	1	1.03±0.03	0.006	96.6 ± 0.7
T4P2	2	2.10 ± 0.11	0.010	96.3 ± 1.4
T4P35	3.5	3.06 ± 0.09	0.022	93.7 ± 1.5
T4PL35	3.5	3.44 ± 0.07	0.011	95.7 ± 1.0
T6P35	3.5	2.86 ± 0.19	0.014	94.9 ± 1.0
T7P35	3.5	3.03 ± 0.05	0.012	94.4 ± 2.2
T10P35	3.5	2.64 ± 0.11	0.020	96.1 ± 1.3

(see Figure S1A) as reported in the literature.[47–49] Lignin has a highly branched structure and lower molecular weight than PANI.[50] As a result, lignin can act as a diluent for PANI by reducing the hydrogen bond interactions between the N-H groups of PANI which has a dispersing effect, favoring the movement of polymer chains. This fact provokes a diminution in the relaxation times of the polymer chains that leads to a diminution in viscosity. Similar behavior was observed previously by Porkodi et al. in polyacrylonitrile and lignin blended solutions.[48] By contrast, no noticeable effect of the photoinitiator concentration on stable shear viscosity, as a function of shear rate, was observed for samples using PANI as filler. This result can be observed in Figure S1B, in which the corresponding graphs remain close throughout the tested range.

2.2. Morphology of the Samples

TEM imaging was performed to analyse the morphology of the lignin, PANI and PANI-L polymers (**Figure 1**).

Lignin particles (Figure 1A) show a circular shape of about 200 nm in diameter. They are probably formed of disordered entangled chains that have shrunk into a "collapsed ball".[44] Concerning PANI doped with HCl, individual PANI nanorods of about 130×35 nm are interwoven and stacked together in dis-

ordered and densely packed aggregates (Figure 1B). When PANI is synthesized in the presence of lignin, similar agglomerates of nanorods are generated but small circular lignin particles are embedded in the interpenetrating network, whose size is much smaller than the original lignin particles. A similar break down of the lignin phase in smaller particles has been reported in the literature in the presence of fillers or resins capable of forming physical and chemical interactions with lignin.[51] Lignin has also a clear dispersing effect on PANI since only in PANI-L samples it is possible to observe individual nanorods, whose surface is partially covered by small spherical lignin particles (Figure 1C).

The morphological differences between the rectangular 3D printed films of pure acrylate resin and the PANI compounds (described in **Table 2**, **Scheme 1**) were evaluated by SEM, as shown in **Figure 2**. Fixing the amount of TPO, as the content of PANI augmented, micropores appeared and the original smooth surface of the pristine acrylic resin became rough due to the increasing agglomeration of PANI clusters [31] (Figure 2).

Moreover, the images of the cryo-fractured cross section of the pure acrylate film show a series of horizontal lines corresponding to the individual layers formed during the printing process (Figure 2A). Upon increasing PANI loading, the perception of the layers in the composites is attenuated and an increase in the features of crack-propagation and porosity is revealed due to the presence of PANI clusters protruding from the cracks and pores (Figure 2B–D). This fact is particularly noticeable in Figure 2D, corresponding to T4P35, the sample with the highest percentage of PANI filler. These images point to poorer interlayer adhesion upon increasing PANI content. These structural features have a negative influence on the mechanical properties (shown in 2.5. section).

However, this tendency is reverted in the composites that used PANI-L as filler (Figure 2E), which suggests better dispersion and integration of PANI clusters within the acrylic resin favored, among other reasons, by the decrease in the viscosity of the liquid monomer mixture. Due to the presence of small spherical lignin particles partially surrounding the PANI nanorods, an uneven and coral like surface is observed in PANI-L aggregates compared to the smoother surface of the PANI aggregates (Insets Figure 2D and 2E). In short, the homogeneity of the samples with PANI-L (T4PL35) clearly improved compared to the composites that included equivalent
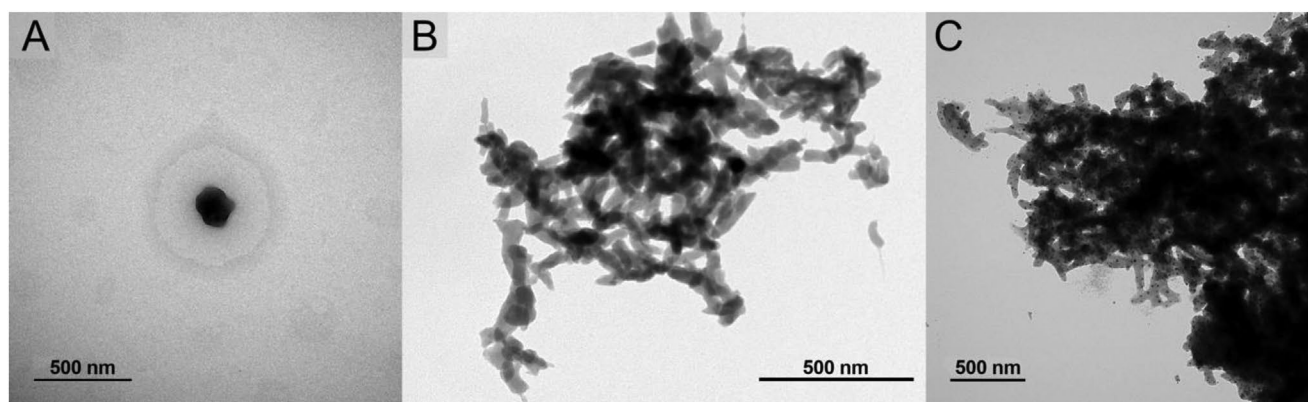
Figure 1. TEM images of A) Lignin, B) pure PANI and C) PANI-L

Table 2. Nomenclature for the developed acrylic composites.

Sample	Filler type	Filler content (wt%)	TPO (wt%)
T4P0	PANI	0	4
T4L04	Lignin	0.4	4
T4P1	PANI	1	4
T4P2	PANI	2	4
T4P35	PANI	3.5	4
T4PL35	PANI-L	3.5	4
T6P35	PANI	3.5	6
T7P35	PANI	3.5	7
T10P35	PANI	3.5	10

*Resin used for all the composites: EGPEA:HDODA 85:15

amounts of PANI (T4P35). This result is promising since porosity in vat polymerization techniques may arise from uncured resin between layers. Interlayer porosity may cause weak interfaces and can affect the overall strength of the printed object.[31,52]

2.3. UV–vis and FTIR spectroscopy

Both UV–vis and FTIR spectra (**Figure 3**A and S2) showed the structural differences between PANI and PANI-L. PANI is present as emeraldine salt form, as demonstrated by the presence of the peaks at 380, 478 (shoulder but clear peak in the first derivative spectrum) and the incomplete band with a maximun at wavelength >810 nm. The first absorption band arises from π-π^* electron transition within benzoid (B) ring, the second and third absorption bands are attributed to the polaron and bipolaron transitions, respectively.[53] The last two bands relate to the doping level and formation of polaron lattice, which represent the protonation stages of PANI chain. Further, the UV–vis absorption spectrum of the PANI-L composite showed a little batochromic shift (the band at 478 nm moved to 485 nm), indicating that lignin in the PANI-L composite slightly increased the π conjugation of PANI, in contrast with the literature.[53]

The presence of Lignin in the PANI-L composite clearly diminishes the strong light absorption around 405 nm, the wavelength applied for DLP. Using the Lambert-Beer law,

Equation (1), it is possible to calculate the absorptivity, ε, at a specific wavelength from the experimental absorbance value (A).[54]

$$A = \varepsilon b c \tag{1}$$

where b is the length of the UV pathway (1 cm) and c is the concentration of the tested material in EGPEA:HDODA dispersion (60, 150 or 250 ppm). The absorptivity of PANI, PANI-L and Lignin at 405 nm was 8.8 l $g^{-1}cm^{-1}$, 5.1 l $g^{-1}cm^{-1}$ and 1.5 l $g^{-1}cm^{-1}$, respectively. As a result of the lower absorptivity of PANI-L, the level of light available for the photoinitiator increases, which may favour the polymerization reaction of its corresponding resin formulation.[54]

The FT-IR spectra of the PANI-L 3D printed composite is plotted in Figure S2 in comparison with those of Lignin and PANI. Analysis of the spectra of lignin [55–57] and PANI [23,29] was based on assignments from the literature. The FTIR spectrum of PANI-L is similar to that of PANI, except for the presence of a new band at 1716 cm^{-1} due to the stretching of C = O lignin groups, shifted towards lower wavenumbers with respect to pure lignin, probably due to the association with the PANI amine groups through the formation of hydrogen bonds. Additionally, other lignin bands, which were overlapped by the PANI signals, can be detected in the difference spectrum (composite spectrum minus normalized PANI, not shown) at 1629, 1228 and 1045 cm^{-1}, that is to say, shifted with respect to pure lignin.

On the other hand, a new band at 3272 cm^{-1}, indicative of hydrogen bond formation between the NH groups (N_{amine} in B rings) of PANI and C = O or OH lignin groups, could only be detected in the difference spectrum. Hydrogen bonding between PANI donor groups and lignin acceptor groups has been described in the literature, parallel to an increase in $-NH^+$ relative to $-N =$ (Quinoid rings) or N_{amine} (Benzenoid) observed by XPS.[56,58] Although no clear shifts are detected, the intensity of the PANI bands at 1300 and 1105 cm^{-1} clearly augmented and the latter band, related to the vibrational mode of protonated amines (δ_{C-H}, $\delta_{Q = N+B/B-NH+, -B}$) and characterizing the delocalization of π electrons, also became broad around 1060–900 cm^{-1}. These changes are also more clearly observed in the difference spectrum and have been ascribed to an interaction between PANI and lignin via π-π stacking and electrostatic interaction.[44,59] All these phenomena show that the introduction
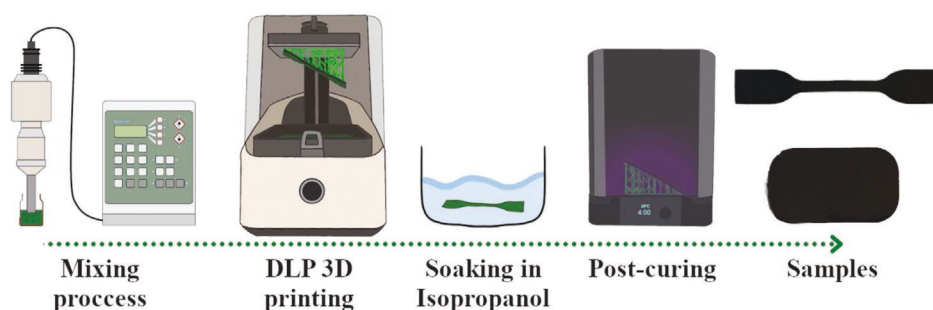

Scheme 1. Diagram of sample preparation
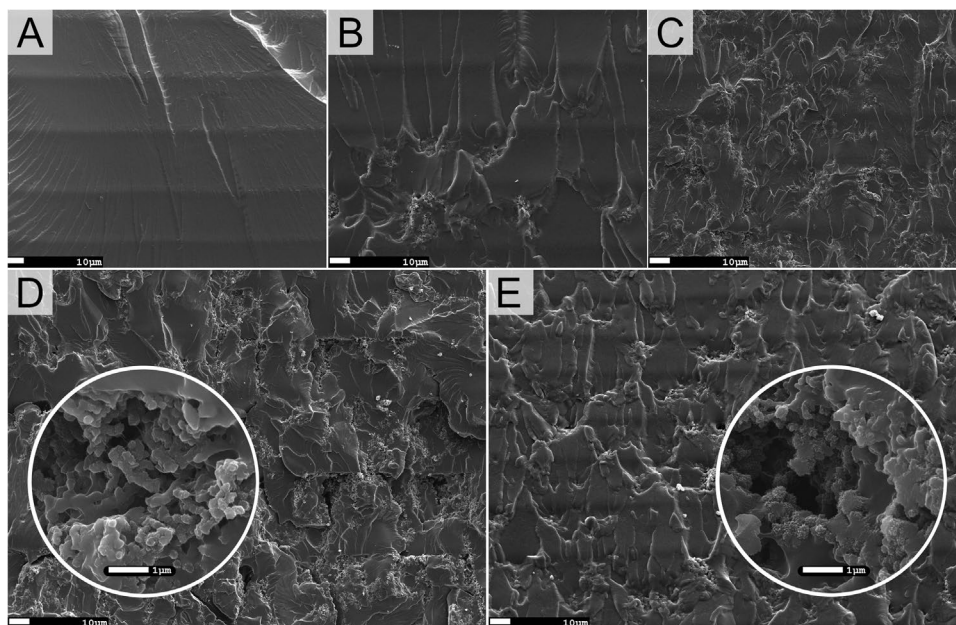
Figure 2. Representative SEM images of A) pure acrylic resin, B) T4P1, C) T4P2 and D) T4P34 and E) T4PL35 with magnitude amplification of 500× and 10000× for the inset.

of lignin not only influenced the structure of PANI, but also revealed interactions between PANI and lignin.

The effects of lignin, PANI, PANI-L and TPO contents on the degree of monomer conversion in the post-cured printed films were studied by ATR-FTIR (Figure S3 and Table 1). The results confirmed a high degree of monomer conversion in both sides of the film of the pristine acrylic matrix (DBC% = 97.9 ± 0.7). By contrast, the DBC% of the printed composites diminished from 96.6% to 93.7% upon increasing PANI content from 1 to 3.5 wt%, while the standard deviations increased due to the greater heterogeneity. Nevertheless, the substitution of PANI for PANI-L 3.5wt% increased the DBC% to 95.7%. This outcome can be explained by the lower light

absorption at 405 nm of PANI-L compared with PANI, that favors the polymerization reaction, as previously discussed. As a result of the greater homogeneity and better inclusion of PANI aggregates within the resin in T4PL35, no PANI bands or new bands ascribed to the H-bonding interaction between the NH groups of PANI and the carbonyl stretching group of the acrylic resin are observed in the spectrum, in contrast with the profile of the spectrum of T4P35 ($\nu_{NH—O=C}$ and $\nu_{C=O—H}$ at 3200 and 1670 cm^{-1}, respectively) (Figure S3). These observations are in agreement with the different morphologies detected by SEM. Similarly, increasing the photoinitiator content from 4 to 10 wt% partly overcomes the competitive strong UV light absorption of PANI and increased the DBC% value
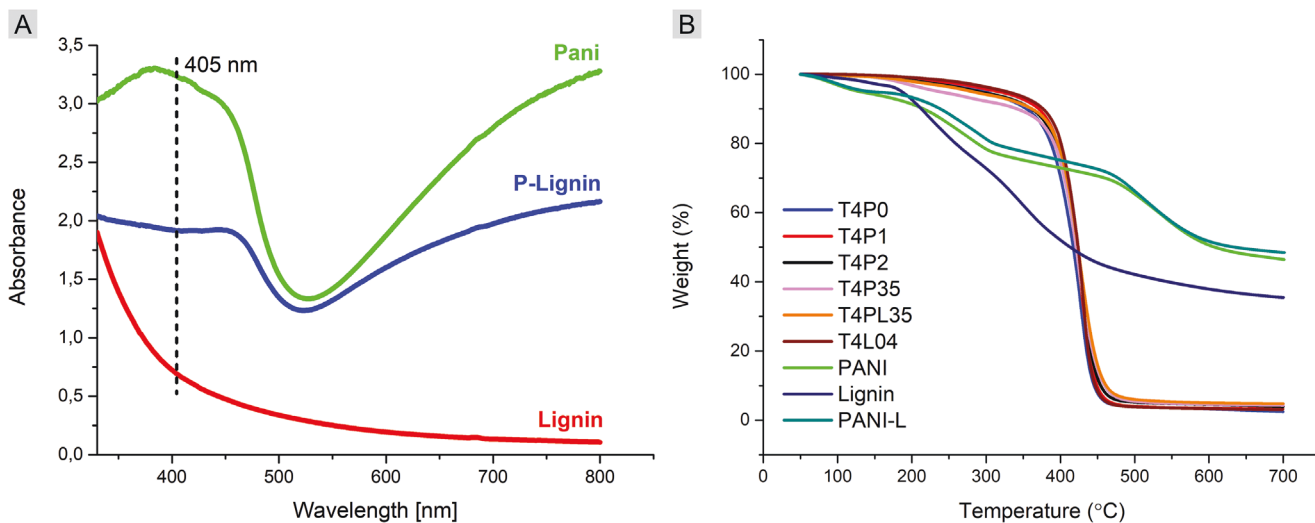
Figure 3. A) UV-visible absorption spectrum of PANI, PANI-L and Lignin in EGPEA:15 wt% HDODA at 250 ppm and B) TGA curves of PANI, Lignin and PANI-L and of the acrylic composites T4P0, T4P1, T4P2, T4P34 and T4PL35.

of the composites with 3.5 wt% PANI,[46,60] in accordance with previous results.

Elemental analysis show that PANI mostly remains in the composite after printing, as the current PANI contents were relatively close to the theoretical amounts, especially for low PANI contents and PANI-L (Table 1). Along with SEM and FTIR results, these data confirm that the use of 3.5wt% PANI-L augmented the amount of the filler embedded within the acrylic matrix compared with 3.5wt% PANI.

2.4. Thermal properties

The thermal behavior of lignin, PANI, PANI-L and the acrylate composites were evaluated by TGA and DSC. The results are displayed in Figure 3B and Table S1. TGA thermograms of lignin, PANI and pristine acrylic matrix are described in detail in the Supplementary Information Section (S1.3).

It is noteworthy that the thermogram of PANI-L is slightly above that of PANI between 100 and 500 °C and that the temperature at which 10% of the total mass is volatilized (T_{10}) increases, which means that the thermal stability of PANI-L is slightly improved with respect to that of PANI. This result has been previously reported, being attributed to an interaction between lignin and PANI chains,[53] as confirmed by FTIR.

In relation with 3D printed acrylic composites, they all apparently exhibit degradation profiles analogous to that of pure acrylic resin, except for the small additional weight loss ascribed to the evaporation of HCl, dopant of PANI. Further analysis indicates that the addition of 0.4% lignin (T4L04) increases T_{10} and T_{onset} by about 5%, while with increasing the amount of PANI the T_{onset} temperatures increase around 7 and 2% for 1 and 2 wt%, respectively. The improved thermal stability is due to the formation of H-bonds between the matrix and both types of fillers.[45,61–63] By contrast, increasing PANI loadings up to 3.5 wt% decreased both T_{10} and T_{onset}, due to the increase in volatiles loss and HCl dopant which is in agreement with the FTIR results. Similar behavior has been observed whenever an acrylic resin is photopolymerized in the presence of strong UV absorbing fillers such as PANI or carbon nanotubes,[5,29,64] which hinders the UV light absorption by the photoinitiator and reduces the effectiveness of the polymerization process.[54]

However, at 3.5% of load, PANI-L shows the opposite effect (T4PL35), increasing both T_{10} and T_{onset} due to the improvement in curing performance, discussed in Section 2.3; thus, the presence of lignin in the filler enables increasing PANI loading without compromising thermal stability.

In line with a previous report,[46] the small variations in the T_g of the printed composites, obtained by DSC, are related with differences in the degree of double bond conversion and, thus, in the crosslinking density (Table S1). Thus, the pure acrylic resin has a T_g around 2°C higher than the values of the composites with 0.4 lignin, 1 and 2 wt% PANI, although the lowest T_g value corresponded to the composite with 3.5 wt% PANI. By contrast, the presence of PANI-L in T4PL35 increases T_g, again due to improved photopolymerization reaction, which increases in DBC%.

Table 3. Influence of sample formulation on the mechanical properties of the printed films measured by tensile test (E = Young's modulus, σ = stress at break and ε = elongation at break).

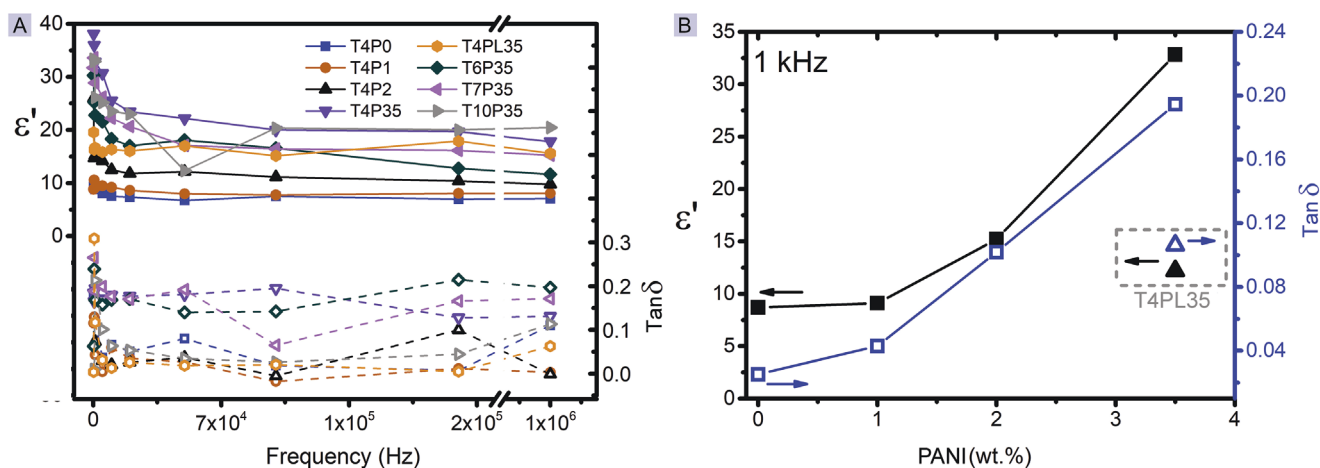| Sample	E (MPa)	σ (MPa)	ε (%)
T4P0	5.4 ± 0.3	1.06 ± 0.11	24.8 ± 2.6
T4L04	4.9 ± 0.2	0.90 ± 0.08	22.6 ± 1.6
T4P1	6.0 ± 0.8	0.73 ± 0.15	16.9 ± 2.8
T4P2	5.4 ± 0.3	0.73 ± 0.05	17.7 ± 0.7
T4P35	6.0 ± 0.6	0.51 ± 0.07	9.8 ± 0.7
T4PL35	6.3 ± 0.6	0.54 ± 0.07	12.2 ± 1.4

2.5. Mechanical properties

To evaluate the practical application of the 3D printed composites, mechanical uniaxial tensile tests till rupture were performed according to ISO 527 with at least five dog-bone shaped specimens, as shown in Figure S4. From the stress–strain curves the modulus, stress at break and elongation at break of the printed composites were calculated and presented in **Table 3**.

In contrast with previous reports,[46,65] no significant differences are observed in the Young modulus of PANI composites compared to pristine acrylic resin within experimental error. However, the tensile strength and the elongation at break, neatly decreased as the amount of PANI increase, reducing ductility (both parameters decreased around 50% for 3.5 wt% PANI). The discrepancies with respect to PANI composites of similar composition [46] may be due to the different experimental protocols. Notwithstanding, the brittle behavior of T4P35 can be attributed to the cracks and pores observed by SEM, mainly located at the interface between layers due to the uncured resin, as is often observed in tray polymerization, especially in heterogeneous compounds.[31,52]

From another point of view, a great number of polymer composite systems have been prepared using lignin as reinforcement.[36,45,66] However, in the present work, a negligible effect on the mechanical properties of the acrylate matrix was observed when only lignin was added. The slight decrease detected in the three mechanical parameters in T4L04, in relation with the pure acrylic matrix, lied within experimental error, which is attributed to the low percentage of lignin included (0.4 wt%). However, when this low content of lignin was added in combination with PANI, namely using the PANI-L composite (T4PL35), the elongation at break increased with respect to T4P35 (~24%). This outcome can be related to the improved dispersion observed by SEM, leading to samples with fewer cracks and pores.

2.6. Electrical properties

The electrical conductivity of the acrylic resin (Figure S5) was $(4.1 \pm 0.1) \times 10^{-11}$ S.m^{-1}, which is similar to that of insulator polymers. This value increased by an order of magnitude with the inclusion of 3.5 wt% PANI, up to $(1.5 \pm 0.1) \times 10^{-10}$ S.m^{-1}. No changes in electrical conductivity, within the experimental

**ADVANCED
SCIENCE NEWS**
www.advancedsciencenews.com

**ADVANCED
MATERIALS
TECHNOLOGIES**
www.advmattechnol.de

Figure 4. Dielectric response of pure acrylate and PANI composites: A) Dielectric constant (ε') and dielectric losses (tan δ) as a function of frequency and B) Dielectric constant (ε') and dielectric losses (tan δ) at 1 kHz for composites with 4 wt% of TPO. For comparison, the values for T4PL35 are displayed inside the gray dotted line square.

error, were observed when increasing the amount of photoinitiator for a fixed amount of PANI of 3.5%, except for T10P35 which decreased slightly (Table S2). When PANI was replaced by PANI-L, there was a slight decrease in the electrical conductivity values, which remained similar to those ofT10P35 and pure acrylic resin. Despite the increase in conductive filler content in the acrylic matrix up to 3.5 wt%, the composites behaved as insulator materials. This is attributed to the PANI electrical percolation threshold within polymer blends, which ranges from 10 to 20 wt% for solvent casting or extruded composites.[67–69] Since amounts of PANI greater than 3.5 wt% hindered the photopolymerization in the 3D printer,[46] the UV curing process of acrylic resins did not allow enough PANI to be added to the monomer solution to achieve the range of semiconductor/conductive materials.

The room temperature dielectric constant (ε') and dielectric losses (tan δ) of the composites are presented in **Figure 4**. The frequency dependence of both parameters for the different PANI/acrylic resin composites are shown in Figure 4A, while Figure 4B displays the dielectric constant and dielectric losses of the samples at 1 kHz. The dielectric constant variation with frequency was similar for all materials, diminishing for low frequencies and then, stabilizing for higher frequencies. The dielectric constant clearly increased with PANI content. At 1 kHz, ε' quadrupled its value upon increasing PANI content from 0 to 3.5 wt% ($\varepsilon' = 7.1 \pm 0.3$ for T4P0 and $\varepsilon' = 32.8 \pm 0.1$ for T4P35) (Table S2).

Regarding the effect of the photoinitiator, the dielectric constant decreased slightly with increasing the photoinitiator content, except for T10P35, in which the dielectric constant augmented for the higher frequencies. The dielectric losses showed a similar behaviour, increasing as the PANI filler in the samples increased, being near tan $\delta \approx 0.03$ for acrylate and tan $\delta \approx 0.19$ for composites with 3.5 wt% PANI at 1 kHz. At 1 kHz (Figure 4B), both dielectric properties presented linear behaviour with respect to PANI content.

When using PANI-L as conductive filler, the dielectric constant was slightly lower than that of the T4P35 sample for high frequencies. However, at low frequencies, the dielectric

constant of this formulation is clearly lower, being less than half the value of the dielectric constant of T4P35 at 1 kHz (from $\varepsilon' = 32.8 \pm 0.1$ for T4P35 to $\varepsilon' = 12.2 \pm 0.8$ for T4PL35). The dielectric constants of all samples at 1 kHz are presented in Table S2. The high dielectric constant for the composite with 3.5 wt% PANI content is attributed to the fact that PANI clusters inside the acrylic matrix produce a significant increase in local electric field when fillers are very close to each other.[70] Thus, the dielectric properties are influenced by the particle distribution and interfacial polarization between the PANI and polymer matrix,[71] enabling the formation of local microcapacitors, and also by the contributions of localized charge with large mobility.[70,72] Therefore, highly improved dielectric properties were achieved using PANI as reinforcement material, increasing the dielectric properties without strong modifications of the electrical conductivity. Hence, the high-dielectric properties[73,74] of the printable acrylates reinforced with 3.5 wt% PANI are ideal for the fabrication of sensors and flexible electronic devices.

2.7. Piezocapacitive measurements

The dielectric properties of PANI/acrylic composites showed strong potential for the development of force transducer arrays, capable of providing a capacitive variation response when subjected to external stimulus such as finger touch or human weight, among others.[3,16] The operation of a piezocapacitive transducer is based on the variation of the capacitance of the materials, typically based on the variation of the distance between the electrodes under pressure.

Piezocapacitance tests were performed measuring both the deformation and capacity of the material as a function of the applied pressure. The changes obtained in capacitance (ΔC) were measured as a function of the applied static load (1, 3, 5, 10, 50 and 100 N of force). The results obtained for T4P35 when varying the force from 10 to 100 N are depicted in **Figures 5**A,B, as illustrative performance of all the acrylic composites with 3.5 wt% PANI and different TPO contents.
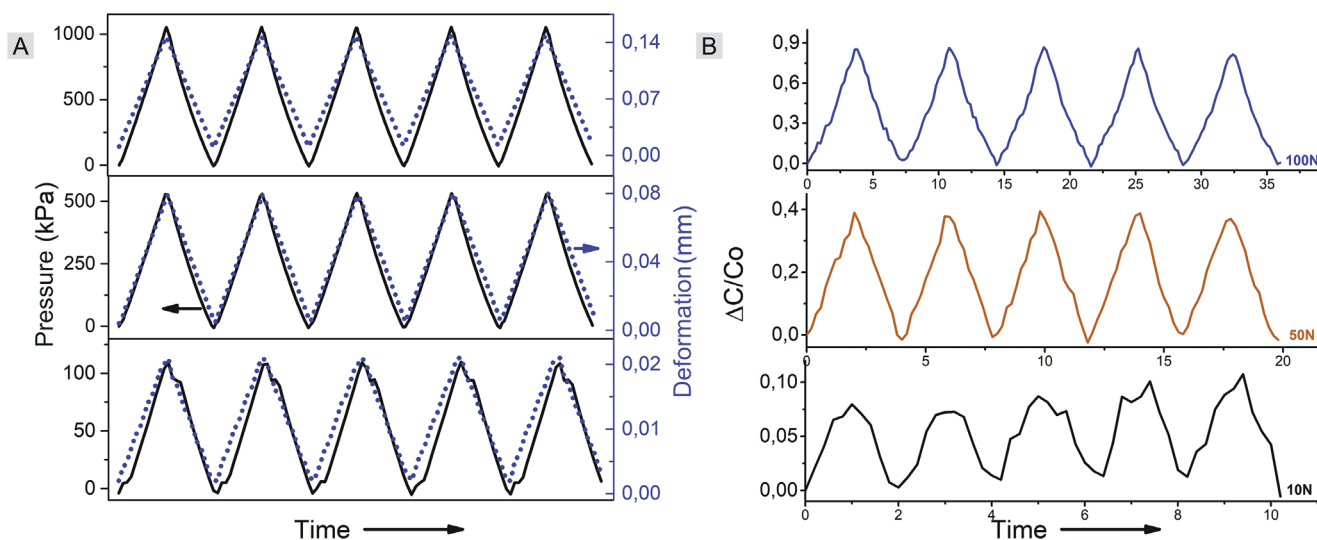
Figure 5. A) Mechanical solicitation and B) capacitive variation response for the T4P35 PANI/acrylic composite. The applied pressure was varied from 100 to 1000 kPa, corresponding to 10–100 N of force. Compression speed was 1 mm min^{-1}.

The sensitivity of a capacitive pressure transducer (S) is defined as $(\Delta C/C_0)/\Delta P$, where ΔC is the capacitance variation of the transducer, C_0 is the capacitance value before applying external pressure and ΔP is the applied pressure.[19] The sensitivities of the composites with 3.5 wt% PANI were thus calculated and shown in **Figure 6**A and Table S3. First of all, the sensitivities of all the assayed samples are similar for the different applied forces from 10 to 100 N, within experimental error. Secondly, in relation with the effect of the photoinitiator content, the sensitivity tends to increase when decreasing the TPO content. Hence, composites with 4 wt% TPO seemed the best candidates for the fabrication of the transducer; for this reason, the limits of the piezocapacitive response of these dielectric materials were further evaluated over a larger range of applied forces (Fig. 6B and Table S3). The sensitivity of T4P35 spans from 11.80 to 0.08 MPa^{-1} in the range of applied forces from 1 N to 200 N, respectively.

From another point of view, the piezocapacitive response of acrylic composites with 3.5 wt% PANI is characterized by an excellent linearity and good sensitivity over the wide range of forces from 1 N to 100 N with no memory effect over 5 cycles. As an example the performance of the pressure transducer made with T4P35 is depicted in Figure 6C,D. The stability and repeatability of this transducer were further confirmed by performing 500 compression and releasing cycling tests in the 0–500 kPa range; as shown in Figure S6 the sensitivity of the composite remained constant, the material returning to its initial shape when the pressure was released.

Furthermore, the transducer developed showed a sensitivity comparable to related sensors based on (PVDF-TrFE-CFE) films[18] or electrospun PVDF nanofiber membrane with carbon nanotubes,[75] but with the advantage that their manufacture using 3D printing is simpler and faster, in addition to being more ecological. Nonetheless, several capacitive pressure sensors with high sensitivity have been reported recently based on porous materials and complicated designs of structure. Generally, bulk composites show lower piezocapacitive sensitivity compared to porous materials[19]; as for hierarchically porous

PDMS composites, variations can be up to three orders of magnitude higher. Highly porous structures show sensitivities near of hundreds of kPa^{-1} but the maximum pressure is lower compared to bulk structures.[76] Further, the dielectric response of the materials is lower, making it difficult processing the output signal.[77] Alternative strategies have been carried out to increase the sensitivity of capacitive pressure sensors such as the addition of fillers of different nature, size and geometry and/or the design of complicated patterns and micro-structured arrays (pyramid, micropillar, microdomes, microcone structures, biomimetic array architecture...), but they typically work under low applied pressures besides the high costs involved in some of these complicated procedures.[77] Opposite to this, the material developed in the present work by a simple and low cost method shows piezocapacitive performance in a very wide range of applied pressures.
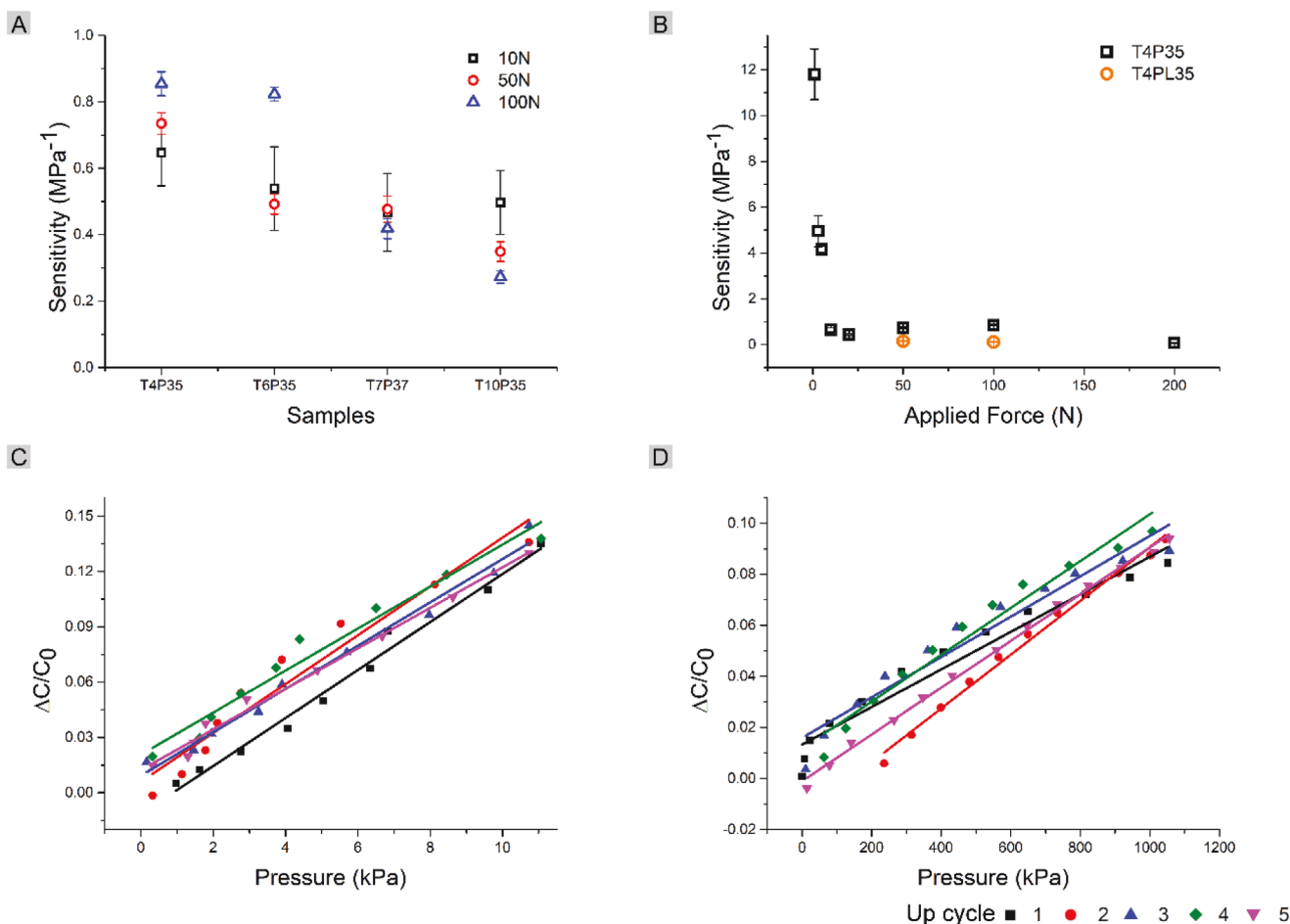
As a final point, the addition of PANI-L, evaluated in T4PL35 for 50 N and 100 N force, showed a decrease in sensitivity compared to the PANI-acrylate compound T4P35 (Figure 6B, Table S3). However, for low-medium pressures, the piezocapacitive response of the sample with lignin is still valid. Moreover, it has the added advantages of improving the dispersion of the conductive filler in the composite and a clear increase in the elongation at break without compromising the sensitivity of the transducer. These reasons justify the choice of this formulation for the development of a new eco-friendly material for the dielectric layer of capacitive pressure sensors.

Based on the versatility and excellent response of the developed materials and considering the potential in the area of 3D printed electronics, a prototype transducer sensor matrix was developed using PANI-L as filler (T4PL35).

2.8. Prototype demonstration

A capacitive pressure transducer device was fabricated by attaching three films of dielectric material (T4PL35) to an

**ADVANCED
SCIENCE NEWS**

www.advancedsciencenews.com

**ADVANCED
MATERIALS
TECHNOLOGIES**

www.advmattechnol.de

Figure 6. A) Piezocapacitive sensitivity of the acrylate composites with 3.5 wt% PANI as a function of the photoinitiator content for applied forces of 10 N, 50 N and 100 N. B) Piezocapacitance sensitivity of the T4P35 sample under loads from 1 N to 200 N and T4PL35 under 50 and 100 N. C) Piezocapacitance sensitivity of T4P35 for applied forces of 0–1 N and D) 0–100 N over 5 cycles.

aluminium foil electrode for the bottom contact. For the capacitor top contact, three aluminium electrodes were glued to the T4PL35 film. The capacitive pressure transducer was connected to the digital pins of the microcontroller (Arduino uno) through a 10 MΩ resistance for signal acquisition (**Figure 7**A and experimental setup in Figure 7B,C). The pressure detection is handled by detection of the logic state of a digital pin connected to the capacitive sensor. As a representative example, the response time and stability under constant force of an individual transducer are illustrated in Figure 7D. PANI-L reinforced resins printed by 3D present stable signal under constant force (either without applied force and after a person of about 80 kg steps on top of the transducer) and a fast response time of about 500 ms ± 200 ms (the error being the minimum response time of the Quadtech measurement equipment).
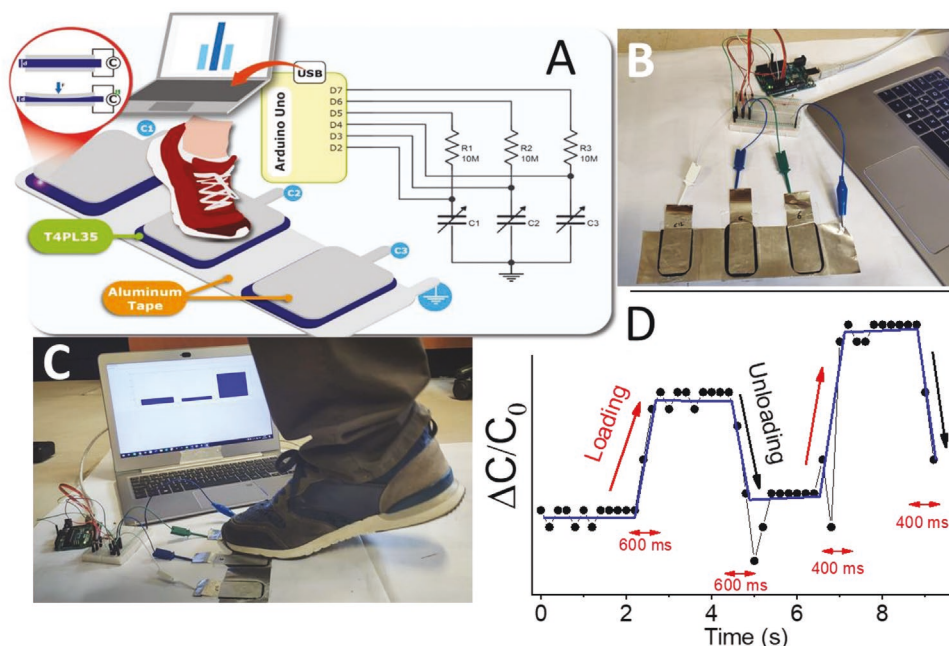
At first, the digital pin connected to the capacitor is pulled to ground, causing the capacitor to discharge through the microcontroller. Next, the microcontroller pulls the pin connected to the resistor to high (5V), counting the time that the logic pin connected to the capacitor switches from low to high. The counting time is proportional to the capacitance variation through pressure variation. The transducers values are fed to

a user interface connected through USB to a laptop computer where the transducers data are shown in a bar chart. The user interface was developed in Python.

The high dielectric PANI-L/resin composite showed excellent capacitive properties for human gait detection. The applied force changed the geometry of the composite materials, decreasing their thickness and increasing the capacitance. Mechanically, the composite fully recovers from the applied forces and can sequentially detect repeated movement (see video in support information). As an example, this material may be used to count the number of persons that cross some specific area, for example in case of emergency evacuation or to control number of people entering events of mass attendance such as sport events or concerts.

3. Conclusion

This work reports on the development of a printable, flexible and wearable pressure sensor consisting of a sustainable photocurable PANI/acrylate resin suitable for DLP. The effects of PANI and TPO contents were first studied; then, the addition

**ADVANCED
SCIENCE NEWS**

www.advancedsciencenews.com

**ADVANCED
MATERIALS
TECHNOLOGIES**

www.advmattechnol.de

Figure 7. Illustration of the piezocapacitive sensor operation, detecting the movement of a human footstep. A) Illustration of the entire system, B) experimental setup, C) walking monitoring and D) response time illustration of individual transducer.

of lignin to the filler as PANI-L was investigated to achieve a low-cost, more eco-friendly composite.

Increasing PANI loading up to 3.5wt% in the composite caused greater porosity, increase in clustering and poorer interlayer adhesion. Moreover, the degree of double bond conversion of the composites decreased compared to the pristine acrylic matrix and the augment in volatiles loss slightly decreased thermal stability. Finally, the mechanical properties were negatively affected, increasing brittleness. Opposite to this, the use of PANI-L instead of PANI at 3.5 wt% clearly improved the homogeneity and ductility of the samples without compromising the thermal stability. The presence of lignin promoted dispersion and integration of PANI clusters within the acrylic matrix, due to the decrease in the viscosity of the liquid monomer mixture and to the lower absorptivity at 405 nm; consequently, the polymerization reaction was favored, facilitating the 3D printing by DLP and improving the quality of the samples.

From another point of view, both composites with either PANI or PANI-L fillers at 3.5 wt% were in the range of insulator materials, as the content of filler was not enough to reach the electric percolation limit. Therefore, these composites seem ideal materials for the manufacture of piezocapacitive sensors as the use of PANI greatly improved the dielectrical properties without significant modifications of the electrical conductivity. The systematic study also revealed that the lowest concentration of TPO assayed (4 wt%) enhanced the signal and sensibility in the capacitive study.

Among all formulations tested, T4P35 presented the best piezocapacitive sensitivity (0.012 kPa^{-1}) in a linear range of 0–10 kPa. The pressure transducers made from this sample showed good capacitive sensing response between 0–2000 kPa (corresponding from 1 to 200 N) and exhibited stable cycling performances (500 cycles) over a wide working pressure regime (0-500 kPa). However, for low-medium range applications, the piezocapacitive response of the sample with lignin is still valid, in addition to being more environmentally friendly. Based on the above considerations and the improvement of the composite properties as a whole, the PANI-L acrylate resin was selected for the fabrication of piezocapacitive prototype transducers suitable for human gait detection. This prototype transducer demonstrated high reproducibility and performance. Hence, it is possible to develop high dielectric constant polymer composites from PANI-L/acrylic resins, allowing an environmental friendlier solvent-free approach for printed electronics and functional materials.

4. Experimental Section

Aniline (ANI, 99.5%) and ammonium persulfate (APS, 99%) were obtained from Sigma-Aldrich (St. Louis, MO, USA) and Acros (Geel, Belgium) respectively. Hydrochloric acid (HCl, 37%) and methanol (MeOH) were purchased from Scharlau (Sentmenat, Spain). Water was purified on an Elix 3 system (Millipore, Molsheim, France). The monomer resin was Ethylene glycol phenyl ether acrylate (EGPEA, molecular weight = 192.21 g mol^{-1}). The crosslinker used for polymer synthesis was 1,6-hexanediol diacrylate (HDODA, molecular weight = 226.27 g mol^{-1}). The photoinitiator was Diphenyl (2,4,6- trimethylbenzoyl) phosphine oxide (TPO, molecular weight = 348.37 g mol^{-1}). Monomer, crosslinker and photoinitiator were purchased from Sigma-Aldrich (St. Louis, MO, USA). 2-Propanol obtained from Scharlau (Sentmenat, Spain) was employed to clean the samples after 3D printing.

Materials and Samples Preparation—Preparation of Lignin: Lignin was extracted from Betula alba bark from an atlantic forest in Ferrol area (northwest of Spain) and subjected to organosolv fractionation. A catalyzed acetic acid process (Acetosolv) was chosen by efficiency reasons due to the acetic group content present in the raw material. In order to adequate the treatment to raw material, the main experimental

**ADVANCED
SCIENCE NEWS**

www.advancedsciencenews.com

**ADVANCED
MATERIALS
TECHNOLOGIES**

www.advmattechnol.de

variables were optimized based on lignin extraction efficiency (data not showed). The final conditions of the acetosolv process applied to the milled samples for lignin release were as follows: 90% acetic acid, 0,2% hydrochloric acid for 55 minutes at atmospheric boiling temperature. The obtained lignin was recovered from acetosolv liquor by water precipitation and lyophilized before its use.

The molecular weight distribution of lignin was characterized by gel permeation chromatography (GPC). A Waters 2695 (Waters, Mildford, MA, USA) system was equipped with a series of linear columns (Styragel 4E and Styragel HR3, 4.6 × 300 mm) and a photodiode array detector (PDA, model 996 UV). The analyses were performed at 35 °C using tetrahydrofuran (THF) as mobile phase at a flow rate of 0.3 mL min^{-1}. Polystyrene standards ranging from 580 to 93800 Da were used for calibration (220 nm). Solutions of lignin in THF (1000 mg L^{-1}) were prepared by gently stirring the samples up to 24 hours. The average of 2 replicates was Mw = 2743, Mn = 1088, polydispersity = 2.5.

Materials and Samples Preparation—Preparation of PANI: PANI was synthetized as previously described in Arias-Ferreiro et al. [29]. The preparation was adapted from the method described by Park et al. [78] and Horta-Romarís et al. [23]. PANI-L was prepared by the polymerization of aniline in the presence of lignin, following a similar procedure. Prior polymerization, 0.8 g of lignin was dispersed in the HCl solution using ultrasonic energy for 1 hour. The polymerization reaction was allowed to proceed for 22 h, under stirring and low temperature in the range 5–10°C. The yield recovered was 5.9 mg.

The elemental analysis of PANI and PANI-L were performed in duplicate on a ThermoFinnigan Flash EA1112 analyser. PANI: 10.92 wt% N; 58.63% C; 5.21% H; 2.4% S; PANI-L: 9.78 wt% N; 55.79% C; 4.77% H; 3.38% S. The C/N atomic ratio derived from these data, 6.26 for PANI and 6.65 for PANI-L, are in agreement with the theoretical value for emeraldine doped PANI ($C_{24}H_{20}N_4Cl_2$) if the counter ion is Cl$^-$. The S/N atomic ratios of 0.10 and 0.15 for PANI and PANI-L, respectively, are associated with the use of APS as oxidant.[46,29,79] Based on the fact that all present nitrogen comes exclusively from PANI, the content of lignin in the PANI-L composite estimated by elemental analysis was 10.4 ± 0.2 wt%.

In order to confirm the last result, the content of lignin in the PANI-L composite was also calculated by UV–vis spectrometry, adapting a method from Zhang et al. [37]. First, samples of ~10 mg of PANI-L composite were extracted with 25 mL of tetrahydrofuran under magnetic stirring up to 24 hours. Tetrahydrofuran is a poor solvent for PANI but a good solvent for lignin. The undissolved material was separated after centrifugation at 5,000 rpm. The concentration of dissolved lignin in the supernatant was determined at 310 nm using a calibration curve function obtained from Organosolv lignin/THF solution at various concentrations (5.2, 10.4, 20.9, 41.7, 104 mg L^{-1}). The sum of 3 consecutive extractions was considered. The experiment was carried out in triplicate and the average result 7.7 ± 0.2 wt%, resembled that of the elemental analysis within the expected differences between techniques.

Materials and Samples Preparation—Preparation and Printing of the Composites: Mixtures were formulated taking as reference previous studies.[29,31] A fixed quantity of the HDODA crosslinker (15 wt%) was mixed with the monomer (EGPEA). Different amounts of conductive filler (PANI and PANI-L,) and photoinitiator (TPO) were added. Composites formulations are shown in Table 2.

The components were placed into vials and sonicated during 30 min using a Digital Sonifier at 15% of intensity (Branson 450) to promote homogeneous dispersion. Just before their use, samples were further mechanically stirred in a Vortex mixer for 2 min at 1000 rpm (VELP Scientific). The formulations were printed with a 3D printer (SLASH PLUS, UNIZ) which employs Digital Light Processing (DLP) printing technology. The printer settings were adjusted based on the printer technical requirements and the composition of the formulations tested. The light irradiation dosage was 76.5 mJ.cm^{-2} for each layer, considering that the light intensity of the 3D printer was 3 mW.cm^{-2} and the exposure time was 25.5 s per layer. The layer thickness was set between 0.05-0.025 mm depending on the formulation. After printing, the samples were soaked in isopropanol during 10 min in order to

remove the non-cured resin. A post-curing process was performed with a post-curing lamp (Form Cure, Formlabs) during 10 min at 35°C. Flexible rectangular films of 50 mm x 35 mm x 0.5 mm and dog-bone shaped specimens according to ISO 527 were prepared to carry out the different tests. The preparation process for 3D printing and the aspect of the composite samples is illustrated in Scheme 1.

The nomenclature and composition of the samples is presented in Table 2.

Sample Characterization: The viscosity of the samples was performed at room temperature using a controlled strain rheometer (ARES, TA Instruments) with parallel-plate geometry (25 mm diameter, 1 mm gap). The steady shear viscosity (η) was measured in a range of shear rates between 0.3 and 100 s^{-1}.

The morphology of lignin, PANI and PANI-L powders was evaluated by transmission electron microscopy (TEM) with JEOL JEM 1010 (80 KeV) equipment after applying 10 mL of the aqueous powder dispersions to a copper grid. The morphology of printed composites was assessed using Scanning Electron Microscopy (SEM). Specimens were broken under cryogenic conditions and examined using a JEOL JSM-7200F Field Emission Scanning Electron Microscope at an accelerating voltage of 10 kV, equipped with an Energy Dispersive X-rays Spectrometry System (EDS) for chemical microanalysis (AZtecLive Nanoanalysis of Oxford Instruments). Prior to observation, the samples were sputter-coated with a thin palladium platinum layer (Cressintong 208HR). The UV–vis spectra of 60, 150 and 250 ppm suspensions of PANI and PANI-L in EGPEA: 15 wt% HDODA were recorded on a Jasco V-750 double-beam UV–vis spectrophotometer between 200 and 800 nm with a sampling interval of 1 nm and 25 accumulations.

The Fourier Transformed Infrared (FTIR) data were recorded on a Jasco 4700 spectrometer equipment. Three absorption spectra of PANI, Lignin and PANI-L were performed in Potassium Bromide (KBr) pellets from 4000 to 400 cm^{-1} and the corresponding average spectra examined. The composite films were analyzed in the Attenuated Reflectance Mode (ATR) by using a MIRacle ZnSe Single Reflection Horizontal ATR accessory. The Fourier Transformed Infrared (FTIR) spectra of the composite films were recorded in the Attenuated Reflectance Mode (ATR) by using a MIRacle ZnSe Single Reflection Horizontal ATR accessory. Three individual spectra were collected on each film between 4000 and 600 cm^{-1}. All the spectra were collected with a 4 cm^{-1} resolution over 64 scans and subjected to baseline and ATR correction. The spectra were analyzed using the Bruker OPUS® software version 5.5. In the post cured printed films, the degree of the acrylate double bonds conversion (DBC%) was calculated from the IR peak area of the band located at 810 cm^{-1}, normalized to the carbonyl ester stretching band ($\nu_{C=O}$) of the acrylic polymer at 1728 cm^{-1}, as internal reference, according to. Equation (2) [54]:

$$DBC\% = \frac{(A_{810} / A_{1728})_{t=0} - (A_{810} / A_{1728})_t}{(A_{810} / A_{1728})_{t=0}} \times 100\% \qquad (2)$$

The elemental analysis of C, H, N, and S of the composites were conducted in duplicate using ThermoFinnigan FlashEA1112 elemental analyser. In order to calculate the experimental wt% of PANI in the printed composites, since PANI is the only compound in the entire mixture that has the nitrogen in its formulation, the experimental wt% of PANI was calculated using Equation (3):

$$Exp\ \%\ Pani = \frac{\frac{Exp\ \%N}{At\ wt\ N}}{Mw\ Pani} \times 100 \qquad (3)$$

Equation (3) is based on the experimental % nitrogen and the molecular weight of PANI (Mw PANI), assuming that PANI molecules were completely protonated (50% oxidized poly(p-phenylene amine imine).[31,80]

Thermogravimetric Analyses (TGA) were performed using a TGA 4000 – Perkin–Elmer set-up under nitrogen atmosphere supplied at a constant flow rate of 50 ml min^{-1}. The composite holders were ceramic

crucibles with a capacity of 60 µL. The cured films were subjected to a heating rate of 10.0 ± 0.1 °C min^{-1} in the temperature range between 50 up to 700 °C. The glass transition temperatures (T$_g$) were evaluated by Differential Scanning calorimetry (DSC) (2010 TA Instruments) under nitrogen atmosphere. 10–12 mg of the composites films were placed in aluminum pans and heated from -40 °C to 200 °C at a rate of 10 °C min^{-1}.

Tensile stress–strain mechanical properties were characterized using an Instron 5569 universal testing machine (Instron Canton, MA) operating at room temperature and at a cross-head speed of 10 mm min^{-1} until failure. At least five dog-bone shaped specimens were tested to measure the tensile properties according to ISO 527.

The electrical and dielectric properties of the samples were measured in volume, with 5 mm of diameter gold electrodes previously deposited on both sides of the sample in a parallel plate configuration using a Polaron SC502 equipment. The electrical resistance (R) of the samples was calculated from the slope of current-voltage (I-V) linear curves obtained with a Keithley 6487 picoammeter/voltage source. The applied voltage was between -10 and +10 V and the corresponding current was measured. Measurements were obtained at two different positions of the samples. Then, the electrical conductivity (σ), inverse of the resistivity (ρ), was determined considering equation (4), where d its thickness of the samples and A is the electrode area.

$$\sigma = \frac{1}{\rho} = \frac{1}{R} \times \frac{d}{A} \tag{4}$$

The capacity (C) and dielectric losses (tan δ) of the samples were obtained with a Quadtech 1920 LCR precision meter in the 200 Hz to 1 MHz frequency range at room temperature. The real part of the dielectric constant (ε') was obtained after equation (5), taking into consideration the parallel plate condenser geometry and the permittivity of vacuum ($\varepsilon_0 = 8.85 \times 10^{-12}$ F m^{-1}).

$$C = \varepsilon' \varepsilon_0 \frac{A}{d} \tag{5}$$

The variation of the capacity under compression, piezocapacitance, was measured using a universal testing machine Shimadzu model AG-IS with load cell of 500 N synchronized with the Quadtech 1920 LCR precision meter. The dielectric response of the different PANI/acrylic composites was measured without and with applied force values of 1, 3, 5, 10, 50 and 100 N.

Supporting Information

Supporting Information is available from the Wiley Online Library or from the author.

Conflict of Interest

The authors declare no conflict of interest.

Data Availability Statement

The data that support the findings of this study are available from the corresponding author upon reasonable request.

[1] C. Mendes-Felipe, J. Oliveira, I. Etxebarria, J. L. Vilas-Vilela, S. Lanceros-Mendez, *Adv. Mater. Technol.* **2019**, *4*, 1800618.

[2] Y. Wang, C. Xing, J. Guan, Y. Li, *Polymers* **2017**, *9*, 562.

[3] T. Marinho, P. Costa, E. Lizundia, C. M. Costa, S. Corona-Galván, S. Lanceros-Méndez, *Compos. Sci. Technol.* **2019**, *183*, 107804.

[4] G. Gonzalez, A. Chiappone, I. Roppolo, E. Fantino, V. Bertana, F. Perrucci, L. Scaltrito, F. Pirri, M. Sangermano, *Polymer* **2017**, *109*, 246.

[5] C. Mendes-Felipe, J. Oliveira, P. Costa, L. Ruiz-Rubio, A. Iregui, A. González, J. L. Vilas, S. Lanceros-Mendez, *Eur. Polym. J.* **2019**, *120*, 109226.

[6] Q. Mu, L. Wang, C. K. Dunn, X. Kuang, F. Duan, Z. Zhang, H. J. Qi, T. Wang, *Addit. Manuf.* **2017**, *18*, 74.

[7] X. Huang, B. Sun, Y. Zhu, S. Li, P. Jiang, *Prog. Mater. Sci.* **2019**, *100*, 187.

[8] I. Cooperstein, E. Sachyani-Keneth, E. Shukrun-Farrell, T. Rosental, X. Wang, A. Kamyshny, S. Magdassi, *Adv. Mater. Interfaces* **2018**, *5*, 1800996.

[9] H. H. Hamzah, S. A. Shafiee, A. Abdalla, B. A. Patel, *Electrochem. Commun.* **2018**, *96*, 27.

[10] W. Zong, N. Chui, Z. Tian, Y. Li, C. Yang, D. Rao, W. Wang, J. Huang, J. Wang, F. Lai, T. Liu, *Adv. Sci.* **2021**, *8*, 2004142.

[11] L. Fertier, H. Koleilat, M. Stemmelen, O. Giani, C. Joly-Duhamel, V. Lapinte, J.-J. Robin, *Prog. Polym. Sci.* **2013**, *38*, 932.

[12] Q. Wang, J. Sun, Q. Yao, C. Ji, J. Liu, Q. Zhu, *Cellulose* **2018**, *25*, 4275.

[13] J. Zhang, P. Xiao, *Polym. Chem.* **2018**, *9*, 1530.

[14] P. J. Bártolo, *Stereolithography Materials, Processes and Applications*, Springer, New York **2011**.

[15] L. S. Ebers, A. Arya, C. C. Bowland, W. G. Glasser, S. C. Chmely, A. K. Naskar, M. P. Laborie, *Biopolymers* **2021**, *112*, 23431.

[16] R. Li, Q. Zhou, S. Bi, S. Cao, X. Xia, A. Yang, S. Li, X. Xiao, *Sens. Actuators, A* **2021**, *321*, 112425.

[17] O. Atalay, A. Atalay, J. Gafford, C. Walsh, *Adv. Mater. Technol.* **2018**, *3*, 1700237.

[18] N. Pereira, S. Gonçalves, J. C. Barbosa, R. Gonçalves, C. R. Tubio, J. L. Vilas-Vilela, C. M. Costa, S. Lanceros-Mendez, *Polymer* **2021**, *214*, 123349.

[19] J. Hwang, Y. Kim, H. Yang, J. H. Oh, *Composites, Part B* **2021**, *211*, 108607.

[20] I. Ragazzini, I. Gualandi, S. Selli, C. Polizzi, M. C. Cassani, D. Nanni, F. Gambassi, F. Tarterini, D. Tonelli, E. Scavetta, B. Ballarin, *Carbohydr. Polym.* **2021**, *254*, 117304.

[21] T. Ali, M. Shah, *Sens. Actuators, A* **2021**, *331*, 113040.

[22] S. Zheng, Y. Jiang, X. Wu, Z. Xu, Z. Liu, W. Yang, M. Yang, *Compos. Sci. Technol.* **2021**, *201*, 108546.

[23] L. Horta-Romarís, M.-J. Abad, M. V. González-Rodríguez, A. Lasagabáster, P. Costa, S. Lanceros-Méndez, *Mater. Des.* **2017**, *114*, 288.

[24] R. Jia, G. Shen, F. Qu, D. Chen, *Energy Storage Mater.* **2020**, *27*, 169.

[25] J. Stejskal, *Polym. Int.* **2019**, *69*, 662.

[26] S. Bhadra, D. Khastgir, N. K. Singha, J. H. Lee, *Prog. Polym. Sci.* **2009**, *34*, 783.

[27] S. Jafarzadeh, P. M. Claesson, P.-E. Sundell, E. Tyrode, J. Pan, *Prog. Org. Coatings* **2016**, *90*, 154.

[28] A. B. Çiğil, E. A. Kandırmaz, H. Birtane, M. V. Kahraman, *Polym. Bull.* **2019**, *76*, 4355.

[29] G. Arias-Ferreiro, A. Ares-Pernas, M. S. Dopico-García, A. Lasagabáster-Latorre, M. J. Abad, *Eur. Polym. J.* **2020**, *136*, 109887.

[30] H. Han, S. Cho, *Polymers* **2018**, *10*, 1003.

[31] G. Arias-ferreiro, A. Ares-pernas, A. Lasagabáster-latorre, N. Aranburu, G. Guerrica-echevarria, M. S. Dopico-garcía, M. J. Abad, *Polymers* **2021**, *13*, 2068.

[32] H. Li, Y. Liang, P. Li, C. He, *J. Bioresour. Bioprod.* **2020**, *5*, 163.

[33] C. M. Ewulonu, X. Liu, M. Wu, H. Yong, *J. Bioresour. Bioprod.* **2019**, *4*, 3.

[34] W. Gao, J. P. W. Inwood, P. Fatehi, *J. Bioresour. Bioprod.* **2019**, *4*, 80.

[35] J. Yang, X. An, L. Liu, S. Tang, H. Cao, Q. Xu, H. Liu, *Carbohydr. Polym.* **2020**, *250*, 116881.

[36] J. T. Sutton, K. Rajan, D. P. Harper, S. C. Chmely, *ACS Appl. Mater. Interfaces* **2018**, *10*, 36456.

[37] S. Zhang, M. Li, N. Hao, A. J. Ragauskas, *ACS Omega* **2019**, *4*, 20197.

[38] F. Ibrahim, D. Mohan, M. S. Sajab, S. B. Bakarudin, H. Kaco, *Polymers* **2019**, *11*, 1544.

[39] X. Feng, Z. Yang, S. Chmely, Q. Wang, S. Wang, Y. Xie, *Carbohydr. Polym.* **2017**, *169*, 272.

[40] J. Zhu, C. Yan, X. Zhang, C. Yang, M. Jiang, X. Zhang, *Prog. Energy Combust. Sci.* **2020**, *76*, 100788.

[41] H. Wang, Y. Pu, A. Ragauskas, B. Yang, *Bioresour. Technol.* **2019**, *271*, 449.

[42] G. Milczarek, O. Inganäs, *Science* **2012**, *335*, 1468.

[43] D. Wang, S. H. Lee, J. Kim, C. B. Park, *ChemSusChem* **2020**, *13*, 2807.

[44] L. Wang, X. Li, H. Xu, G. Wang, *Synth. Met.* **2019**, *249*, 40.

[45] V. K. Thakur, M. K. Thakur, P. Raghavan, M. R. Kessler, *ACS Sustainable Chem. Eng.* **2014**, *2*, 1072.

[46] G. Arias-ferreiro, A. Ares-pernas, A. Lasagab, N. Aranburu, G. Guerrica-echevarria, M. S. Dopico-garc, *Polymers* **2021**, *13*, 2068.

[47] H. C. Liu, C. C. Tuan, A. A. Bakhtiary Davijani, P. H. Wang, H. Chang, C. P. Wong, S. Kumar, *Polymer* **2017**, *111*, 177.

[48] P. Porkodi, J. K. Abhilash, H. K. Shukla, J. Rawat, *Polym. Bull.* **2020**, *77*, 3937.

[49] J. Roman, W. Neri, V. Fierro, A. Celzard, A. Bentaleb, I. Ly, J. Zhong, A. Derré, P. Poulin, *Nano Today* **2020**, *33*, 100881.

[50] L. Horta-Romarís, M. V. González-Rodríguez, A. Lasagabáster, F. Rivadulla, M. J. Abad, *Synth. Met.* **2018**, *243*, 44.

[51] N. A. Nguyen, C. C. Bowland, A. K. Naskar, *Appl. Mater. Today* **2018**, *12*, 138.

[52] J. R. C. Dizon, A. H. Espera, Q. Chen, R. C. Advincula, *Addit. Manuf.* **2018**, *20*, 44.

[53] Z. W. He, Q. F. Lü, J. Y. Zhang, *ACS Appl. Mater. Interfaces* **2012**, *4*, 369.

[54] S. Jafarzadeh, M. Johansson, P. E. Sundell, M. Claudino, J. Pan, P. M. Claesson, *Polym. Adv. Technol.* **2013**, *24*, 668.

[55] J. J. Villaverde, J. Li, M. Ek, P. Ligero, A. De Vega, *J. Agric. Food Chem.* **2009**, *57*, 6263.

[56] J. H. Seo, C. S. Choi, J. H. Bae, H. Jeong, S. H. Lee, Y. S. Kim, *BioResources* **2019**, *14*, 9169.

[57] M. Wen, Y. Zhao, Z. Li, S. Lai, Q. Zeng, C. Liu, Y. Liu, *Diam. Relat. Mater.* **2021**, *111*, 108219.

[58] Z. Deng, T. Hu, Q. Lei, J. He, P. X. Ma, B. Guo, *ACS Appl. Mater. Interfaces* **2019**, *11*, 6796.

[59] D. Yang, W. Huang, X. Qiu, H. Lou, Y. Qian, *Appl. Surf. Sci.* **2017**, *426*, 287.

[60] O. A. de Raponi, L. C. M. Barbosa, B. R. de Souza, A. C. Ancelotti Junior, *Adv. Polym. Technol.* **2018**, *37*, 3579.

[61] A. Mirmohseni, A. Gharieh, M. Khorasani, *Iran. Polym. J.* **2016**, *25*, 991.

[62] B. H. Chengyue Ge, Xiaogang Yang Cheng Li, *J. Appl. Polym. Sci.* **2012**, *123*, 627.

[63] S. Hajirahimkhan, C. C. Xu, P. J. Ragogna, *ACS Sustainable Chem. Eng.* **2018**, *6*, 14685.

[64] S. N. A. Ramlan, W. J. Basirun, S. W. Phang, D. T. C. Ang, *Prog. Org. Coatings* **2017**, *112*, 9.

[65] H. Joo, S. Cho, *Polymers* **2020**, *12*, https://doi.org/10.3390/polym12010067.

[66] X. You, X. Wang, H. J. Zhang, K. Cui, A. Zhang, L. Wang, C. Yadav, X. Li, *ACS Appl. Mater. Interfaces* **2020**, *12*, 39892.

[67] L. Horta Romarís, M. V. González Rodríguez, B. Huang, P. Costa, A. Lasagabáster Latorre, S. Lanceros-Mendez, M. J. Abad López, *J. Mater. Chem. C* **2018**, *6*, 8502.

[68] P. Costa, J. Oliveira, L. Horta-Romarís, M.-J. Abad, J. A. Moreira, I. Zapiráin, M. Aguado, S. Galván, S. Lanceros-Mendez, *Compos. Sci. Technol.* **2018**, *168*, 353.

[69] X. Wu, C. Lu, X. Zhang, Z. Zhou, *ACS Appl. Mater. Interfaces* **2014**, *6*, 21078.

[70] C. W. Nan, Y. Shen, J. Ma, *Annu. Rev. Mater. Res.* **2010**, *40*, 131.

[71] A. Poudel, A. Coffey, J. Kennedy, S. Lyons, K. Thomas, P. Walsh, *Int. J. Mater. Mech. Manuf.* **2015**, *4*, 237.

[72] C. Mendes-Felipe, J. C. Barbosa, S. Gonçalves, N. Pereira, C. M. Costa, J. L. Vilas-Vilela, S. Lanceros-Mendez, *Compos. Sci. Technol.* **2020**, *199*, 108363.

[73] A. Siddiqui, R. Y. Khosa, M. Usman, *J. Mater. Chem. C* **2021**, *9*, 5055.

[74] M. P. Kim, C. W. Ahn, Y. Lee, K. Kim, J. Park, H. Ko, *Nano Energy* **2021**, *82*, 105697.

[75] X. Yang, Y. Wang, X. Qing, *Sens. Actuators, A* **2019**, *299*, 111579.

[76] Q. Liu, Y. Liu, J. Shi, Z. Liu, Q. Wang, C. F. Guo, *Nano-MicroLett.* **2022**, *14*, https://doi.org/10.1007/s40820-021-00770-9.

[77] J. Chen, L. Li, Z. Zhu, Z. Luo, W. Tang, L. Wang, H. Li, *Mater. Today Chem.* **2022**, *23*, 100718.

[78] H.-W. Park, T. Kim, J. Huh, M. Kang, J. E. Lee, H. Yoon, *ACS Nano* **2012**, *6*, 7624.

[79] S. J. Tang, A. T. Wang, S. Y. Lin, K. Y. Huang, C. C. Yang, J. M. Yeh, K. C. Chiu, *Polym. J.* **2011**, *43*, 667.

[80] Y. Yang, W. Yang, *Polym. Adv. Technol.* **2005**, *16*, 24.